Respiratory Research

RESEARCH

Open Access

Ferritinophagy mediated by the AMPK/ULK1 pathway is involved in ferroptosis subsequent to ventilator-induced lung injury

Huajin Ou[1,2,3,4†], Jinyuan Lin[1,2,3,4†], Liu Ji[1,2,3,4†], Liu Ye[1,2,3,4], Maoyao Ling[1,2,3,4], Xiaoting Liao[1,2,3,4], Fei Lin[1,2,3,4], Yuqing Wang[1,2,3,4], Bijun Luo[2,3,4,5], Zhaokun Hu[1,2,3,4] and Linghui Pan[1,2,3,4*]

Abstract

Mechanical ventilation (MV) remains a cornerstone of critical care; however, its prolonged application can exacerbate lung injury, leading to ventilator-induced lung injury (VILI). Although previous studies have implicated ferroptosis in the pathogenesis of VILI, the underlying mechanisms remain unclear. This study investigated the roles of ferritinophagy in ferroptosis subsequent to VILI. Using C57BL/6J mice and MLE-12 cells, we established both in vivo and in vitro models of VILI and cyclic stretching (CS)-induced cellular injury. We assessed lung injury and the biomarkers of ferroptosis and ferritinophagy, after appropriate pretreatments. This study demonstrated that high tidal volumes (HTV) for 4 h enhanced the sensitivity to ferroptosis in both models, evidenced by increased intracellular iron levels, lipid peroxidation and cell death, which can be mitigated by ferrostatin-1 treatment. Notably, nuclear receptor coactivator 4 (NCOA4)-mediated ferritinophagy contributed to ferroptosis in VILI. Inhibition of autophagy with 3-methyladenine or NCOA4 knockdown decreased intracellular Fe^{2+} levels and inhibited lipid peroxidation, thereby attenuating CS-induced lung injury. Furthermore, it has also been observed that the AMPK/ULK1 axis can trigger ferritinophagy in VILI. Collectively, our study indicated that MV can induce ferroptosis by promoting NCOA4-dependent ferritinophagy, which could be a novel therapeutic target for the prevention and treatment of VILI.

Keywords Ventilation-induced lung injury, Ferroptosis, Ferritinophagy, AMPK-ULK1 axis

Introduction

The high morbidity and mortality of acute respiratory distress syndrome (ARDS) is a major medical challenge worldwide [1, 2]. Mechanical ventilation (MV) is a critical intervention for patients with acute respiratory failure and other severe conditions [3, 4]. Despite its life-saving potential, MV can paradoxically induce or exacerbate lung injury, a condition referred to as ventilator-induced lung injury (VILI) [5]. VILI poses a significant threat to patient outcomes by initiating lung biotrauma, subsequently inducing systemic inflammation, and potentially contributing to multi-organ failure—a prevalent cause of mortality in patients with ARDS [6]. However, its

†Huajin Ou, Jinyuan Lin and Liu Ji these authors contributed equally to this work and share first authorship.

*Correspondence:
Linghui Pan
panlinghui@outlook.com
[1]Department of Anesthesiology, Guangxi Medical University Cancer Hospital, He Di Rd No.71, Nanning 530021, P. R. China
[2]Guangxi Engineering Research Center for Tissue & Organ Injury and Repair Medicine, Nanning, China
[3]Guangxi Health Commission Key Laboratory of Basic Science and Prevention of Perioperative Organ Disfunction, Nanning, China
[4]Guangxi Clinical Research Center for Anesthesiology, Nanning, China
[5]Department of Anesthesiology, The Maternal and Child Health Care Hospital of Guangxi Zhuang Autonomous Region, Nanning, Guangxi, China

detailed underlying mechanisms of VILI remain incompletely understood.

Ferroptosis is a novel type of iron-dependent nonapoptotic cell death different from apoptosis, necrosis, and autophagy. It's triggered by a combination of iron toxicity, lipid peroxidation, and plasma membrane damage [7, 8]. Ferroptosis is intricately regulated by iron metabolism, lipid metabolism, and mitochondrial function. Glutathione peroxidase 4 (GPX4), acyl-CoA synthase long-chain family member 4 (ACSL4), and solute carrier family 7 member 11 (SLC7A11) are the key regulators of ferroptosis [9–13]. Dysregulation of ferroptosis can disrupt immune responses and has been implicated in various pathological conditions [8]. Autophagy activation has been shown to elevate intracellular iron levels by degrading ferritin, thereby leading to oxidative damage through the Fenton reaction, known as ferritinophagy [14]. Nuclear receptor coactivator 4 (NCOA4) is a selective cargo receptor mediating ferritinophagy, namely the cytosolic iron storage complex. NCOA4-mediated ferritinophagy maintains intracellular iron homeostasis by facilitating ferritin iron storage or release [15]. Ferritinophagy levels are controlled by NCOA4 levels, which in turn are regulated by cellular iron levels [16]. In our previous studies, a notable relationship between ferroptosis and VILI has been established [17, 18]. This finding provides crucial insights into the integral role of ferroptosis in VILI. However, the detailed underlying mechanism of ferritinophagy in VILI-induced ferroptosis remains largely unknown. Therefore, the present study focused on ferritinophagy in VILI and unraveled its potential mechanisms.

Recent studies have suggested that autophagy, particularly ferritinophagy, plays a crucial role in the regulation of ferroptosis. Infection and inflammation can promote iron chelation into cells [14]. Accumulating evidence has shown that ferritinophagy is implicated in the development and progression of various pathological processes and diseases, including lung injury, neurodegeneration, and cardio-vascular diseases [19–22]. Adenosine 5'-monophosphate (AMP)-activated protein kinase (AMPK) is a key regulator of cellular energy homeostasis and, plays a significant role in the regulation of autophagy. It is expressed in various metabolism-related organs and can be activated by various stimuli [23]. ULK1, a critical regulator of autophagy, plays a major role in autophagy [24]. It has been found that the mtROS-AMPK-ULK1 signaling pathway is probably involved in regulating the zinc oxide nanoparticles-induced ferroptosis of endothelial cells [25]. Bisphenol A regulates iron-autophagy-mediated death in renal tubular epithelial cells through the AMPK/mTOR/ULK1 signaling pathway [26]. In addition, AMPK/ULK1 axis-mediated activation of autophagy and NCOA4-mediated degradation of ferritin by autophagy has been linked to PM2.5-induced ferroptosis of fibrotic cells [27]. However, whether the AMPK/ULK1 signaling pathway is involved in NCOA4-mediated ferritinophagy in VILI has not been investigated.

In this study, we investigated the role of ferritinophagy in VILI and unraveled its underlying mechanisms. We revealed that ventilator-induced autophagy was essential for NCOA4-dependent degradation of ferritin, which was directly linked to ventilator-induced ferroptosis of VILI in vivo and CS-induced damage of MLE12 cells. Furthermore, we found that the AMPK/ULK1 signaling pathway regulated this process. Intriguingly, our findings also revealed that ferrostatin-1 can mitigate VILI and ferritinophagy by inhibiting ferroptosis. Hence, our study provided novel insight into the molecular mechanisms of VILI and highlighted ferritinophagy as a promising target for treatment.

Materials and methods

Reagents

3-Methyladenine (3-MA), compound C, and Phen green SK (PGSK) diacetate were obtained from MedChemExpress company (Shanghai, China). Selective inhibitor of ferroptosis Ferrostain-1 (Fer-1) was procured by Targetmol (Shanghai, China). Enzyme-linked immunosorbent assay (ELISA) kits for the quantification of tumor necrosis factor-alpha (TNF-α), interleukin-6 (IL-6), and interleukin-1 beta (IL-1β) were purchased from YouPin Biological Technology Co. Ltd (Shenzhen, China). Tissue Iron Content Assay Kit was purchased from Solarbio (Beijing, China). Assay kits for detecting total protein, Lyso-Tracker Green, and malondialdehyde (MDA) were purchased from Beyotime Biotech (Shanghai, China). BODIPY™ 581/591 C11 and cell counting Kit-8 (CCK8) were obtained from GLPBIO (Montclair, CA, USA). FerroOrange was obtained from Donjido (Shanghai, China). GPX4 (sc-166570, Santa Cruz Biotechnology), SLC7A11 (12509, Affinity), NCOA4 (A5695, ABclonal), FTH1 (R23306, Zenbio), AMPK (340763, Zenbio), P-AMPK (R380431, Zenbio), ULK1 (381887, Zenbio), p-ULK1 (80218-1-RR, Proteintech), β-actin (4970, Cell Signaling Technology), and GAPDH (sc-137179, Santa Cruz Biotechnology) were used as primary antibodies. Goat anti-rabbit IgG H&L (ab216773) was purchased from Abcam (Cambridge, MA, USA). The goat anti-Mouse IgG H&L (92632210) was provided by LI-COR (NE, USA). HRP-conjugated Affinipure goat anti-rabbit lgG (H + L) was obtained from Proteintech (Wuhan, Chain). Cy3-labeled goat anti-rabbit IgG (GB21303) and Cy3 Labeled Goat Anti-Mouse IgG (GB21301) were purchased from Servicebio Technology (Wuhan, China). The specific primers of SLC7A11, GPX4, and NCOA4 were synthesized and provided by Sangon Biotech (Shanghai, China).

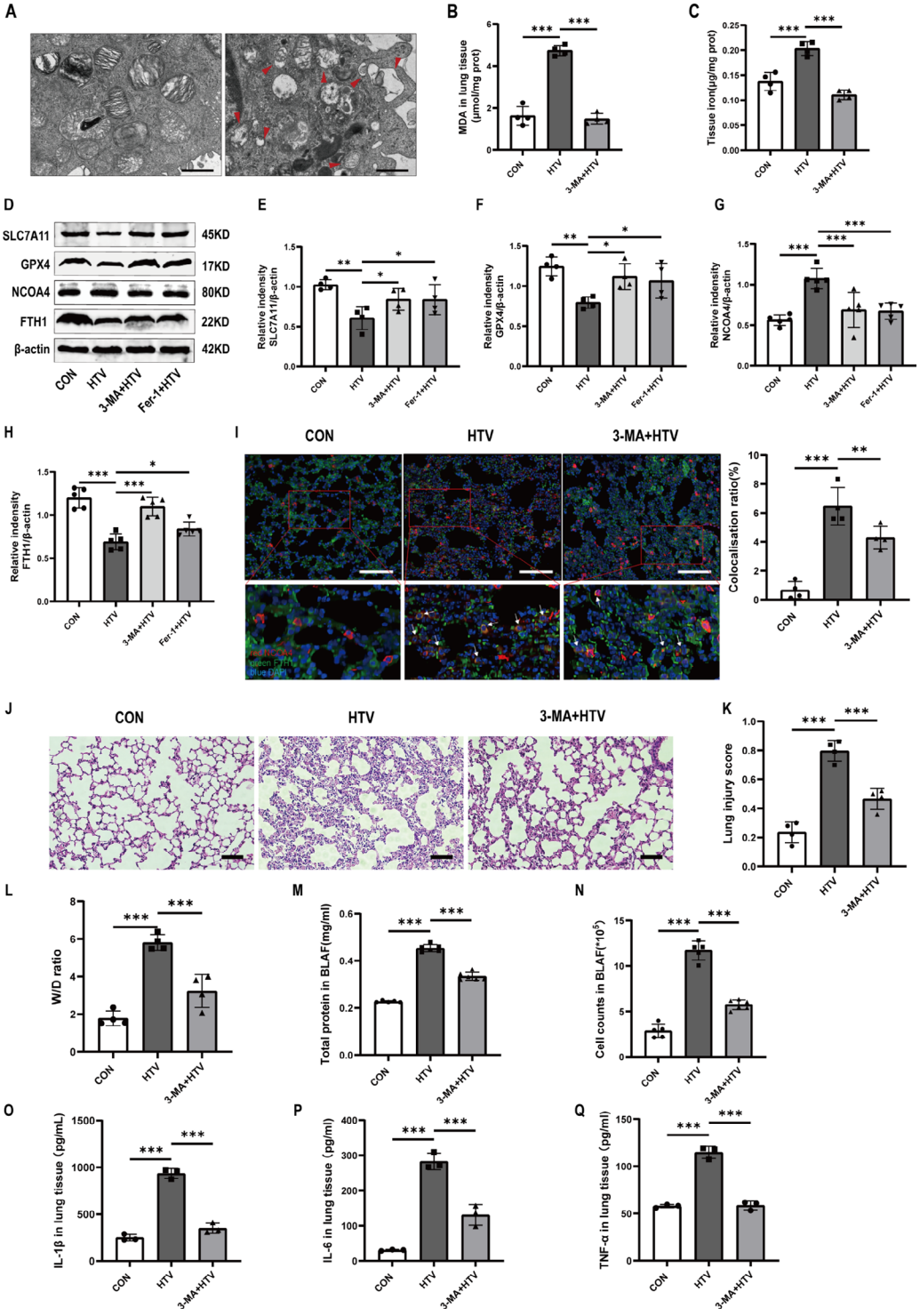

Fig. 1 Ferritinophagy participated in ventilator-induced ferroptosis in vivo. (**A**) TEM images depict lung tissue sections from both groups. Obvious autophagosomes were found in the HTV group. Red arrows represent autophagosome. Magnifications: 6000 X and acceleration voltage: 80 KV. Scale bar: 1 μm. (**B**) MDA levels in lung tissues ($n = 4$). (**C**) The iron content in the lung tissues of mice ($n = 4$). (**D**) Representative Western blotting bands for SLC7A11, GPX4, NCOA4, FTH1, and β-actin in lung tissues. (**E-H**) Relative protein expression of SLC7A11, GPX4, NCOA4, and FTH1 to β-actin ($n = 4$). (**I**) Immunofluorescence assay demonstrated that the co-localization of FTH1 and NCOA4 significantly increased in the HTV group compared to other groups. Scale bar: 100 μm. The percentage of co-localization between FTH1 and NCOA4 was quantified using ImageJ Fiji software ($n = 4$). (**J**) H&E staining was performed on tissue samples from both groups, with a scale bar indicating 100 μm. (**K**) Pathological scoring was conducted based on the H&E staining results ($n = 4$). (**L**) Wet/Dry ratios of lung tissue ($n = 4$). (**M**) Total protein concentrations in BALF ($n = 6$). (**N**) Infiltrating cell counts in BALF ($n = 6$). (**O-Q**) The levels of IL-1β, IL-6, and TNF-α in lung tissue ($n = 3$). Data are expressed as mean ± SD. "*" indicates significant difference between groups (*$p < 0.05$, ** $p < 0.01$ or *** $p < 0.001$)

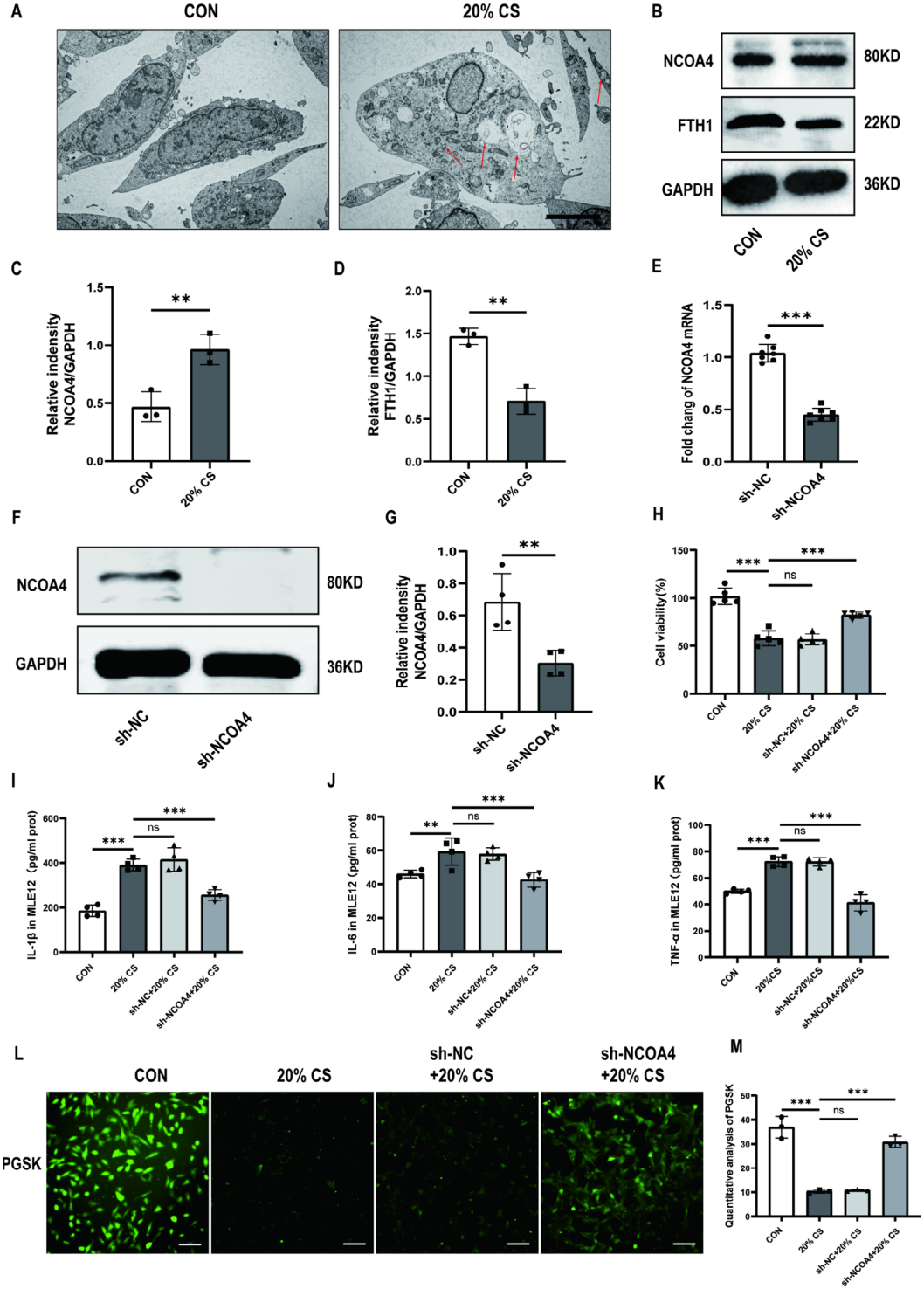

Fig. 2 Ferritinophagy promotes ventilator-induced ferroptosis of MLE-12 cells through ferritin degradation mediated by NCOA4. (**A**) Representative TEM images of MLE12 cells untreated or treated with 20% CS. Red arrows represent autophagosomes. Magnifications: 5000 X, acceleration voltage: 80 kV. Scale bar: 5.0 μm. (**B**) Representative Western blotting bands of NCOA4, FTH1, and GAPDH in MLE12 cells. (**C**, **D**) Relative protein expression of NCOA4 and FTH1 was divided into GAPDH ($n = 3$). (**E**) The mRNA levels of NCOA4 knockdown in MLE12 cells ($n = 7$). (**F**) Representative Western blotting images of NCOA4 and GAPDH in MLE12 cells. (**G**) The protein expression of NCOA4 relative to GAPDH ($n = 4$). (**H**) Cell viability was detected using a CCK8 assay ($n = 5$). (**I-K**) Levels of IL-1β, IL-6, and TNF-α in MLE12 cells ($n = 4$). (**L**) PGSK probe staining for Fe^{2+} in MLE12 cells with different treated groups. Scale bar: 100 μm. (**M**) Quantification of the fluorescence intensity of PGSK using ImageJ Fiji software ($n = 3$). Data are expressed as mean ± SD. "*" indicates significant differences between groups (*$p < 0.05$, ** $p < 0.01$ or *** $p < 0.001$)

Establishment of the VILI model in mice

Male C57/BL6 mice (25 ± 2 g, 6–8 weeks old) were purchased from the Animal Center of Guangxi Medical University (Nanning, China). Mice were conditioned under controlled conditions at a room temperature of 22 °C ± 2 °C with a 12-hour light/dark cycle. They had ad libitum access to standard diet and tap water. Mice were randomly allocated into five groups: (1) control group (CON group, spontaneous breathing post-intubation, 4 h); (2) high tidal volume group (HTV group, MV with high tidal volume, 20 ml/kg, 4 h); (3) Fer-1 + HTV group [Fer-1 (1 mg/kg) was intraperitoneally injected for 14 consecutive days before MV (20 ml/kg for 4 h)] [17]; (4) 3-MA + HTV group [3-methyladenine (3-MA) (35 mg/kg) was intraperitoneally injected 1 h before MV (20 ml/kg) for 4 h), once] [28]; (5) compound C + HTV group [compound C, (20 mg/kg), intraperitoneally, once, 1 h before MV (20 ml/kg) for 4 h] [29]. The animal model of VILI was successfully established based on our previous study [30, 31]. At the end of MV or spontaneous breathing, mice were euthanized via intraperitoneal administration of a high dose of anesthetics. Subsequently, lung tissue, blood serum, and bronchoalveolar lavage fluid (BALF) samples were obtained for subsequent experimental analysis. All animal experiments were conducted with utmost care to minimize the inflammatory response.

Histopathological analysis

Hematoxylin and eosin staining were used to measure the pathological changes in the lungs of mice with VILI. The lung tissue was fixed in 4% paraformaldehyde and subsequently embedded in paraffin. Then, tissue blocks were sliced into 4 μm-thick sections and affixed onto slides. Following deparaffinization, the sections were meticulously stained with hematoxylin and eosin (H&E) before a thorough examination under a light microscope. As previously reported, the degree of lung injury was measured based on a histologic ALI scoring system [32, 33].

Immunofluorescence (IF) staining

Immunofluorescence staining was conducted as previously described [22]. Briefly, dewaxed paraffin sections were subjected to immunofluorescent staining after a sequence of deparaffinization and rehydration. The tissues were incubated at 4℃ overnight with SLC7A11 (1:200), GPX4 (1:200), NCOA4 (1:200) and FTH1 (1:200) primary antibodies. Cy3-labeled goat anti-rabbit IgG (1:400) or Cy3-labeled goat anti-mouse IgG (1:400) was used as fluorophore-conjugated secondary antibodies. The nucleus was stained with DAPI. Subsequently, the fluorescently stained lung tissue samples were examined under a fluorescent microscope (Nikon EclipseC1, Nikon).

Inflammatory responses

The wet/dry (W/D) weight ratio was calculated to crudely assess VILI lung edema. The middle lobe of the right lung was weighed (wet weight) and placed in an oven at 60 °C for 48 h (dry weight). The pulmonary permeability of mice with VILI was evaluated by measuring total protein levels in BALF supernatant using a bicinchoninic acid (BCA) assay. Cells in BLAF were counted using a hemocytometer to determine the inflammatory infiltration of VILI mice. Thereafter, the serum levels of mouse IL-1β, mouse IL-6, and mouse TNF-α were quantified using ELISA kits following the manufacturer's instructions.

Measurement of tissue iron and malondialdehyde (MDA) concentrations

Iron and MDA concentrations in lung tissues were measured to investigate the levels of ferroptosis. Lung iron measurement was conducted using the Tissue Iron Content Assay Kit (BC4355, Solarbio, Beijing, China). MDA levels were measured using the Lipid Peroxidation MDA Assay Kit (S0131, Beyotime, Shanghai, China) following the manufacturer's protocol.

Generation of an in vitro model of VILI

Mouse lung epithelial cells (MLE12) were cultured in Dulbecco's modified Eagle's medium (DMEM) supplemented with 10% fetal bovine serum (FBS) and 1% penicillin/streptomycin (Invitrogen, USA). MLE12 cells were cultured with 5% CO_2 at 37 °C. To stably knock-down the NCOA4 gene in MLE12 cells, we used plasmids LV2N (U6/Puro)-Ncoa4-1130-mus and LV2N (U6/Puro)-NC purchased from GenePharma (Suzhou, China) as shRNA targeting NCOA4. We employed Lipofectamine 2000 Transfection Reagent (Invitrogen, 11668030) to transduce the target plasmid and helped plasmid into 293T cells for virus production. Finally, puromycin was utilized to select positive cells. Subsequently, we successfully established an in vitro model of VILI based on our previous published study [17, 34]. Briefly, cells in the logarithmic growth phase were seeded onto six-well Bio-Flex plates (Flexcell International) at standard densities. Following a 24-hour incubation, cells were exposed to cyclic stretching (CS) using the FX 6000TM Tension Plus system equipped with a 25 mm loading station (Flexcell International, McKeesport, PA, United States). The stretching was applied at a rate of 30 cycles per minute (0.5 Hz), with an equal stretch and relaxation phase and a sine wave pattern. In our study, the pathological CS was conducted at 20% changes in basement membrane surface area corresponding to 80% of total lung capacity. Cells were stretched for 4 h at 37°C in a humidified incubator containing 5% CO_2. The entire experimental procedure was meticulously controlled by computer software. In addition, the culture medium was supplemented with

10 μmol/L of compound C to inhibit AMPK [29]. Culture supernatants and cells were obtained after 4 h of cell stretching treatment.

Cell viability assay

Cell viability was determined using the CCK-8 assay kit. After treatment, cells were seeded at a density of 1 × 10^4 cells per well onto 96-well plates for 12 h. Subsequently, the CCK-8 solution was added directly to the culture medium and incubated at 37 °C for 2 h. Finally, using a microplate reader, the optical density values were detected at 450 nm.

Transmission electron microscopy (TEM)

TEM assays were conducted as previously described [17]. Lung tissues were collected after modeling and then cut into 1–2 mm cubes, fixed in 2.5% glutaraldehyde and 2.5% paraformaldehyde in 0.1 M sodium cacodylate buffer (pH 7.4) for at least 2 h at 4 ℃. Next, cubes were put into the same buffer with 2% uranyl acetate for 2 h at room temperature before dehydration in graded alcohols and propylene oxide. After embedding in resin, the samples were cut into ultrathin slices, stained with uranyl acetate and observed using a HT7800 transmission electron microscope (Hitachi, Japan). Similarly, MLE12 cells were harvested for TEM analysis to evaluate cellular damage and the detailed structure of autophagosomes.

Measurement of intracellular iron

Intracellular iron levels were measured using Phen Green SK (PGSK) [35]. MEL12 cells were seeded at onto plates after pretreatment, washed with PBS, and dark incubated with 20 μM PGSK for 20 min at 37 ℃. The results were visualized using fluorescence microscopy (Leica, Germany).

Lipid peroxidation assay

Suitably treated cells were incubated with 10 μM BODIPY™ 581/591C11 fluorescence probe for 30 min in a humidified incubator (37 ℃, 5% CO_2). Nuclear staining was conducted with DAPI, followed by washing with PBS. Finally, the results were visualized using fluorescence microscopy (Leica, Germany).

Localization of intracellular and lysosomal Fe^{2+}

Suitably treated cells were co-stained with FerroOrange (1 μM) and Lyso-Tracker Green (100 nM) in a serum-free medium. They were incubated in an incubator with 5% CO_2 at 37 °C for 30 min. Cells were washed with PBS. The results were immediately observed using fluorescence microscopy (Leica, Germany).

Real-time PCR

The mRNA levels of NCOA4, SLC7A11, and GPX4 were determined using real-time PCR with specific primers under Real-Time PCR System as detailed in previously. The primer sequences were as follows:

SLC7A11, forward: 5′-ATGGTCAGAAAGCCAGTTG TG-3′, reverse: 5′-GCTCCAGGGCGTATTACGAG-3′;

GPX4, forward: 5′-CTCCGAGTTCCTGGGCTTGT G-3′, reverse: 5′- CCGTCGATGTCCTTGGCTGAG-3′;

NCOA4, forward: 5′-AGTTCCTTGTCAGAGTGGCT TATGG-3′, reverse: 5′-ACCCAGTCGGCAGTGTTAAA GG-3′;

β-actin, forward: 5′-CCACGACAAGGAGCTGCTTC TG-3′, reverse: 5′-ACCCTGTCCGCCATCACATCA-3′;

GAPDH, forward: 5′-CCTTCATTGACCTCAACTA CATGG-3′, reverse: 5′-CTCGCTCCTGGAAGATGGT G-3′;

β-actin and GAPDH were used as internal controls. We employed the $2^{-\triangle\triangle Ct}$ method for quantification.

Western blotting

Total proteins were extracted from the lung tissue and MLE12 cells using radio-immunoprecipitation assay (RIPA) buffer supplemented with protease inhibitor and protein concentrations were assessed using BCA protein assay kit. Then, equal amounts of protein and the molecular weight marker were added to the lanes of sodium dodecyl sulfate (SDS)-polyacrylamide gel. They were subsequently transferred onto polyvinylidene fluoride (PVDF) membranes. After being blocked with Western blotting rapid blocking buffer for 30 min at room temperature, the membranes were incubated by SLC7A11 (1:700), GPX4 (1:200), NCOA4 (1:1000), FTH1 (1:1000), AMPK (1:500), P-AMPK (1:500), ULK1 (1:500), P-ULK1 (1:1000), and β-actin (1:1000), and GAPDH (1:1000) primary antibodies. Next, they were incubated with the following secondary antibodies: goat anti-rabbit IgG H&L (1:15000) or goat anti-Mouse IgG H&L (1:20000). Finally, Western blotting bands were visualized using an Odyssey two-color infrared laser imaging system (LICOR, USA).

Statistical analyses

SPSS 26.0 software (IBM, USA) was used for statistical analysis. All data are presented as mean ± standard deviation (SD). Differences were analyzed using Analysis of Variance (ANOVA) followed by the LSD-t test and the SNK test for pair-wise comparisons. *P* value less than 0.05 was considered statistically significant.

Results

Ferroptosis was activated during VILI

In our prior research, we have demonstrated the occurrence of ferroptosis during VILI [17]. To further investigate the role of ferroptosis in VILI, we administered

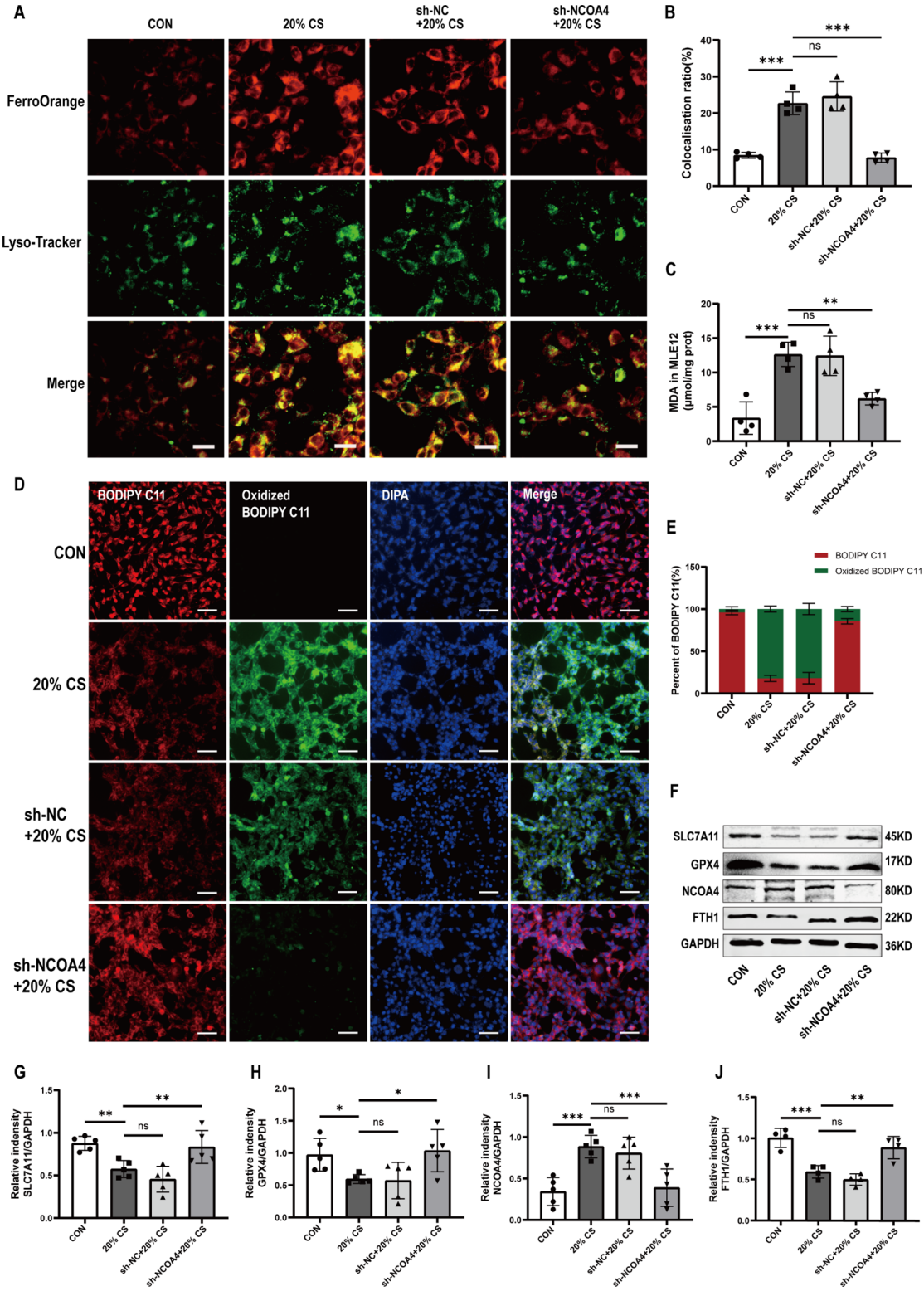

Fig. 3 Knockdown NCOA4 contributed to reducing ferroptosis caused by ferritinophagy in MLE-12 cells with cyclic overstretching. (**A**) Immunofluorescence images of the co-localization of intracellular and lysosomal Fe^{2+}. Scale bar: 20 μm. (**B**) Quantification of the fluorescence intensity of FerroOrange co-localized with Lyso-Tracker Green by ImageJ Fiji software ($n = 4$). (**C**) MDA levels in MLE12 cells ($n = 4$). (**D**) Immunofluorescence images of C11-BODIPY in MLE12 cells. Scale bar: 50 μm. (**E**) Percent of the fluorescence intensity of BODIPY C11 and oxidized BODIPY C11 measured by ImageJ Fiji software. (**F**) Representative Western blotting images of SLC7A11, GPX4, NCOA4, FTH1, and GAPDH in MLE12 cells. (**G**-**J**) Relative protein expression levels of SLC7A11, GPX4, NCOA4 and FTH1 to GAPDH ($n = 5$). Data are expressed as mean ± SD. "*" indicates significant difference between groups (*$p < 0.05$, ** $p < 0.01$ or *** $p < 0.001$)

an in vivo study where the ferroptosis inhibitor Fer-1 was administered to the MV with HTV group. Pretreatment with ferrostatin-1 significantly alleviated lung injury (Supplementary Fig. 1), indicating that ferroptosis was activated during VILI and exacerbated the lung damage. Concurrently, we established an in vitro model using MLE12 cells to further investigate the role of ferroptosis in VILI. We subjected the cells to 20% CS and included a no-stretch control group to assess cell injury. Our findings revealed that cyclic overstretching induced cell injury and triggered ferroptosis in MLE12 cells (Supplementary Fig. 2). Collectively, these results suggested that ferroptosis is activated during VILI both in vivo and vitro.

Ferritinophagy participated in ventilator-induced ferroptosis in vivo

Ferroptosis is currently considered an autophagy-dependent cell death. The pharmacological inhibitor of autophagy 3-MA was applied in clarify the relationship between ferritinophagy and ferroptosis in VILI mice. The results of TEM showed that treatment with HTV increased the number of autophagic vacuoles (autophagosomes) compared to the CON group (Fig. 1A). As expected, MDA (Fig. 1B) and iron content (Fig. 1C) measurement in lung tissue showed that compared with the HTV group, 3-MA inhibited HTV-induced upregulation of lipid peroxidation and iron overload in mice. Autophagy-dependent ferroptosis, also known as ferritinophagy, is the autophagic degradation of ferritin which depends on the selective cargo receptor NCOA4. Cellular ironis primarily sequestered within ferritin, a protein complex consisting of 24 subunits made up of both ferritin light (FTL) and heavy (FTH1) chains [36]. Western blotting revealed that HTV downregulated FTH1, but upregulated NCOA4. 3-MA significantly increased the expression levels of FTH1, SLC7A11, and GPX4 and decreased the expression levels of NCOA4, suggesting that inhibition of autophagy ameliorated ventilator-induced ferroptosis in mice (Fig. 1D-H). Interestingly, western blotting showed that treatment with Fer-1 also downregulated the levels of NCOA4 and upregulated the levels of FTH1. An obvious co-localization of FTH1 and NCOA4 was detected by immunofluorescence analysis in the HTV group (Fig. 1I). These data indicated that NCOA4 mediated autophagy-dependent ferroptosis in VILI mice. At the same time, we used H&E staining and lung injury scores to detect lung tissue structure, which indicated that compared to the control group, 3-MA decreased the alveolar wall thickness and resulted in alveolar collapse, poor structure alveolar septal edema, thickening, and massive inflammatory cell infiltration (Fig. 1J, K). Similarly, W/D ratio (Fig. 1L), total protein level (Fig. 1M) and infiltrated cell counts (Fig. 1N) in lung tissue show that treatment with 3-MA ameliorated HTV-induced edema and prevented inflammatory cell infiltration. Furthermore, the plasma levels of inflammatory factors, including IL-1β, IL-6, and TNF-α, were consistent with the histopathological changes (Fig. 1O-Q). Collectively, these results revealed that ferritinophagy participated in ventilator-induced ferroptosis in vivo and inhibition of autophagy ameliorated ventilator-induced ferroptosis and lung injury in mice.

Ferritinophagy promoted ventilator-induced ferroptosis of MLE-12 cells through ferritin degradation mediated by NCOA4

Ferritinophagy is a new type of autophagy that depends on the selective cargo receptor NCOA4 [14]. We next investigated whether ferritinophagy is activated in MLE12 cells after 4 h of 20% CS. Firstly, TEM images indicated that cells in the 20% CS group had an increased number of autophagosomes compared to cells in the control group (Fig. 2A). 4 h of 20% CS enhanced the protein expression levels of NCOA4 and decreased FTH1 levels in MLE12 cells (Fig. 2B-D). These results suggested that the overstretching of MLE12 cells activated ferritinophagy. Then, we stably knocked down the NCOA4 gene in MLE12 cells using a lentiviral infection system (Fig. 2E-G). Subsequently, the results showed that NCOA4 knockdown markedly relieved 4 h of 20% CS induced cellular injury, as evidenced by increased cell viability (Fig. 2H). The cellular levels of inflammatory factors, including IL-1β, IL-6, and TNF-α were consistent with changes in cell viability (Fig. 2I-K). Similarly, 20% CS decreased the cellular intensity of PGSK, which was reversed by NCOA4 knockdown. (Fig. 2L, M). We used intracellular Fe^{2+} and lysosomal colocalization assay to illuminate the regulatory role of NCOA4 in the activation of ferroptosis and iron overload in 20% CS-induced cellular injury. The colocalization of intracellular and lysosomal Fe^{2+} was lower in the sh-NCOA4 + 20% CS group compared to the 20% CS group. These findings suggest that iron overload was alleviated after NCOA4 knockdown (Fig. 3A, B). Furthermore, we found that NCOA4 knockdown inhibited MDA production (Fig. 3C) and lipid peroxidation (Fig. 3D, E) compared to the 20% CS group. Our results showed that proteins associated with ferroptosis, like SLC7A11 and GPX4, were significantly suppressed after treatment with 20% CS for 4 h. Similarly, ferritinophagy-related protein NCOA4 markedly downregulated with FTH1 was upregulated under the same condition. However, these changes were significantly reversed by NCOA4 knockdown (Fig. 3F-J). In summary, these findings suggested that NCOA4-mediated ferritinophagy induced the ferroptosis of cyclic overstretching in MLE12 cells.

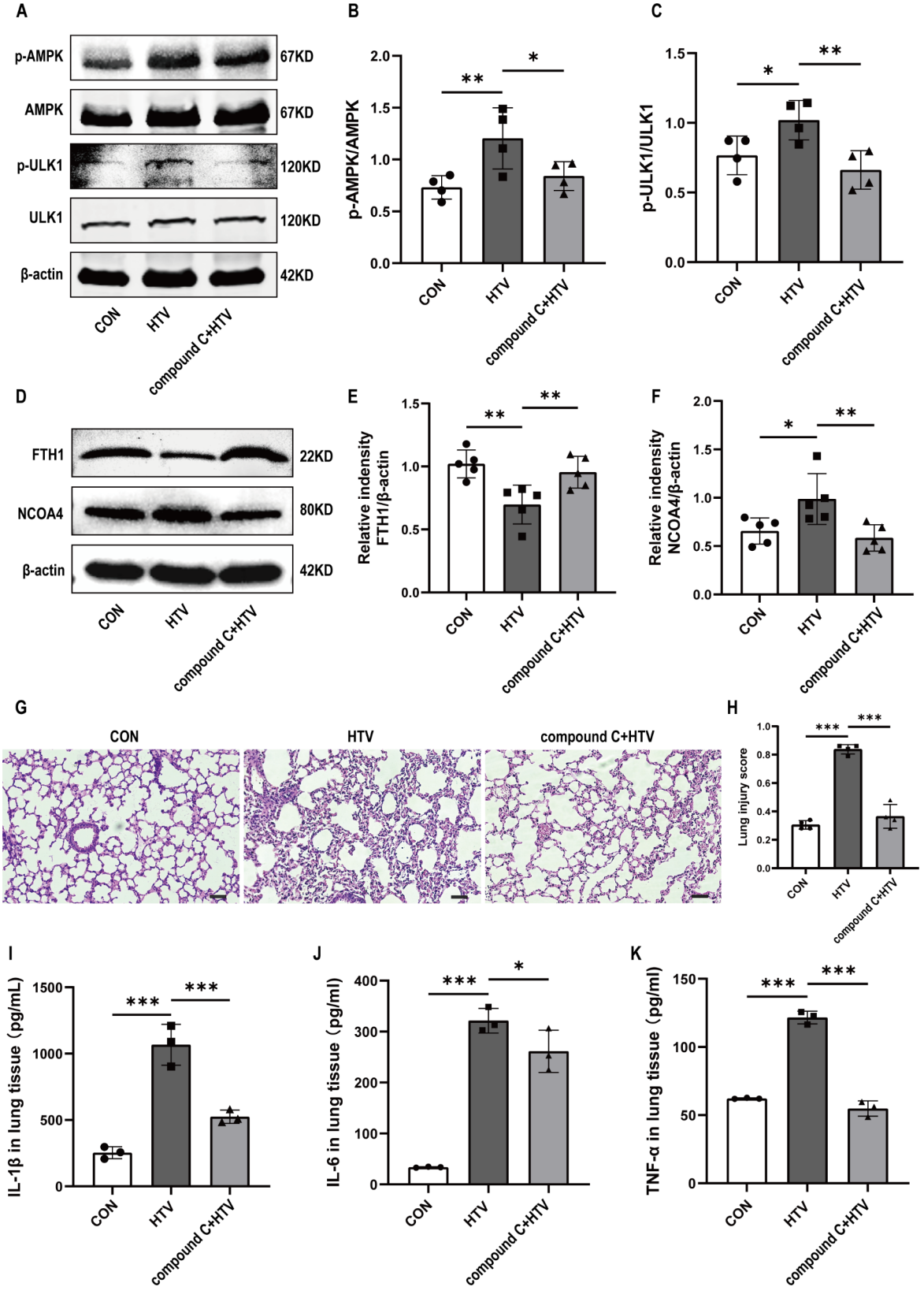

Fig. 4 (See legend on next page.)

(See figure on previous page.)

Fig. 4 The AMPK/ULK1 axis was involved in the activation of ferritinophagy activation induced by ventilator-induced lung injury in mice. (**A**) Representative Western blotting images of p-AMPK, AMPK, p-ULK1, ULK1, and β-actin in lung tissues. (**B**) The protein expression of P-AMPK relative to AMPK ($n = 4$). (**C**) The protein expression of P-ULK1 relative to ULK1 ($n = 4$). (**D**) Representative Western blotting images of FTH1, NCOA4, and β-actin in lung tissues. (**E**, **F**) The protein expression of FTH1 and NCOA4 relative to β-actin ($n = 5$). (**G**) H&E staining was performed on tissue samples from both groups, with a scale bar indicating 100 μm. (**H**) Pathological scoring was conducted based on the H&E staining results ($n = 4$). (**I**) IL-1β levels in lung tissue ($n = 3$). (**J**) IL-6 levels in the lung tissue ($n = 3$). (**K**) TNF-α levels in the lung tissue ($n = 3$). Data are expressed as mean ± SD. "*" indicates significant difference between groups (*$p < 0.05$, ** $p < 0.01$ or *** $p < 0.001$)

The AMPK/ULK1 axis is involved in the activation of ferritinophagy induced by ventilator-induced lung injury in mice

We next investigated the pathways involved in ventilator-induced activation of ferritinophagy. AMP-activated protein kinase (AMPK) is involved in autophagy by activating unc-51-like autophagy activating kinase 1 (ULK1) [37]. Western blotting indicated that p-AMPK and p-ULK1 were slightly upregulated in the HTV group. Pretreatment with compound C significantly reduced the phosphorylation of AMPK and ULK1, which reversed the expression trends of these proteins in the HTV group. This indicates that the AMPK pathway is involved in ventilator-induced activation of autophagy (Fig. 4A-C). We found that compound C significantly increased the protein levels of FTH1 and decreased the protein levels of NOCA4 in the HTV group (Fig. 4D-F). Furthermore, the results showed that compound C ameliorated lung injury, which was characterized by decreased lung tissue damage (Fig. 4G, H) and reduced levels of inflammatory cytokines (Fig. 4I-K). Collectively, these findings indicated that ventilator induced autophagy-dependent ferroptosis via the AMPK pathway.

The AMPK-ULK1 axis is involved in ferritinophagy activation induced by cyclic overstretching in vitro

To confirm that cyclic overstretching-induced autophagy was activated via the AMPK/ULK1 pathway, we measured the expression of proteins related to this pathway by Western blotting. Similar to in vivo findings, in vitro results, indicated that the protein expression levels of p-AMPK and p-ULK1 were markedly upregulated by exposure to 20% CS for 4 h (Fig. 5A-C). Notably, compound C markedly decreased the expression of p-AMPK and p-ULK1, reversed the degradation of FTH1, upregulated the expression levels of NCOA4 (Fig. 5D-F), and ameliorated cell injury (Fig. 5G-I). Taken together, our results suggested that the AMPK/ULK1 axis aggravated damage and ferritinophagy in cells under 20% CS.

Discussion

Atelectasis, edema, alveolar instability, and subsequent hypoxemia in a severely injured lung may lead to respiratory failure, necessitating mechanical ventilation and subsequent VILI [5, 38]. VILI is a major complication of intensive care [39], which activates inflammatory mediators and leads to the overproduction of inflammatory cytokines, local injury, and even multi-organ dysfunction. Although significant progress has recently been made in understanding the pathogenesis of this disease, clinically available treatments are still limited. Current effective treatments for VILI mainly include regulating the tidal volume, oxygen concentration and positive end-expiratory pressure [38–40]. However, the results are still unsatisfactory. Previous studies have discovered that necroptosis [41], apoptosis [42], and autophagy [43] are involved in the pathogenesis of VILI. However, the mechanism of VILI is not yet fully elucidated. Therefore, it is of great significance to investigate the pathogenesis and treatment of VILI.

Ferritinophagy was first described by Mancias et al. in 2014 [15]. Using quantitative proteomics, they identified NCOA4 as a selective autophagy receptor that mediates ferritin degradation in autophagosomes, and leads to the releases of Fe^{2+}. Ferritinophagy is closely associated with various physiological and pathological processes in normal conditions. It is closely regulated by an iron-dependent protein network that maintains the intracellular Fe^{2+} balance and the related physiological functions [16]. However, excessive ferritinophagy can lead to ferroptosis. Ferroptosis is an iron-dependent cell death associated with lipid peroxidation, mitochondrial dysfunction, and activation of autophagy [7]. Many studies have demonstrated that ferritinophagy is an upstream pathway for ferroptosis in many diseases [44, 45]. A recent study reported that regulation of NCOA4-mediated iron recycling ameliorates paraquat-induced lung injury by inhibiting ferroptosis [9]. Melatonin alleviates septic ARDS by inhibiting NCOA4-mediated ferritinophagy in alveolar macrophages [46]. However, whether ferritinophagy contributes to ventilator-induced ferroptosis remains unclear.

In our previous studies, we have established the relationship between ferroptosis and VILI, indicating that Ferrostatin-1 significantly alleviates ventilator-induced lung injury by inhibiting ferroptosis in mice. In the present study, we explored the relation association of ferritinophagy with ventilator-induced ferroptosis. Surprisingly, 3-MA, an autophagy inhibitor inhibited ventilator-associated ferroptosis in mice. We measured ferritinophagy-related indicators, and revealed that MDA and iron overload were reduced in the lung tissue after treatment with 3-MA. Consistent with these findings, SLC7A11, GPX4, and FTH1 were significantly upregulated and

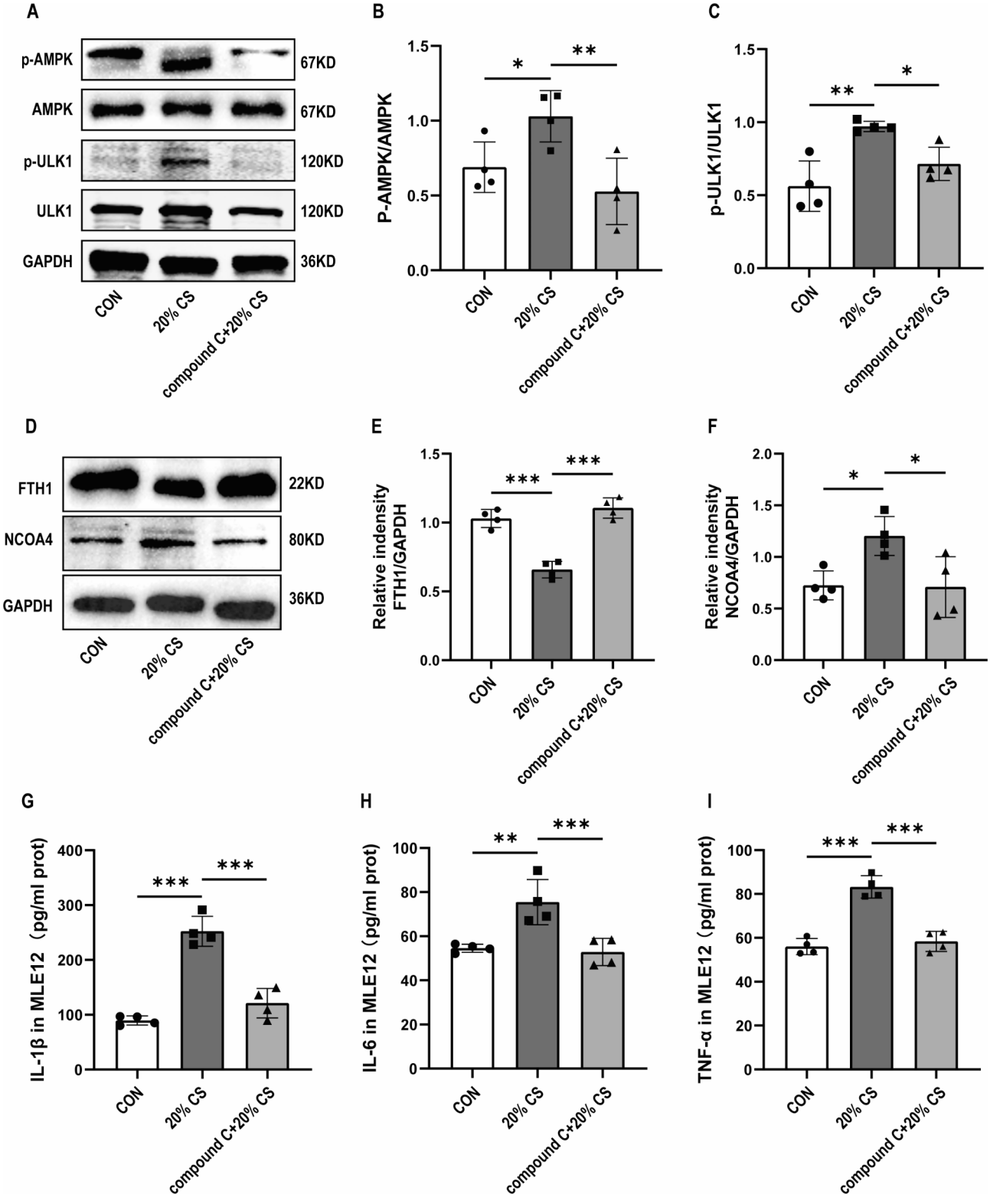

Fig. 5 The AMPK-ULK1 axis is involved in ferritinophagy activation induced by cyclic overstretching in vitro. (**A**) Representative Western blotting images of p-AMPK, AMPK, p-ULK1, ULK1, and GAPDH in MLE12 cells. (**B**) The protein expression levels of p-AMPK relative to AMPK ($n = 4$). (**C**) The protein expression of p-ULK1 relative to ULK1 ($n = 4$). (**D**) Representative Western blotting images of FTH1, NCOA4, and GAPDH in MLE12 cells. (**E**, **F**) Relative protein expression of FTH1 and NCOA4 relative to GAPDH ($n = 4$). (**G-I**) The levels of IL-1β, IL-6, and TNF-α in MLE12 cells ($n = 4$). Data are expressed as mean ± SD. "*" indicates significant difference between groups (*$p < 0.05$, ** $p < 0.01$ or *** $p < 0.001$)

NCOA4 was downregulated after pretreatment with 3-MA. Notably, Fer-1 or 3-MA pretreatment ameliorated ferroptosis-related events in vivo, indicating that inhibition of iron may act as a promising approach for treating VILI. In vitro, we demonstrated that similar to the effect of 3-MA, NCOA4 knockdown suppressed cells damage, intracellular iron overload, and lipid peroxidation of the cyclic overstretching. Thus, NCOA4-dependent selective ferritinophagy was shown to be involved in cellular Fe^{2+} overload induced by 20% CS for 4 h. We explored the co-localization of Fe^{2+} and lysosomes by fluorescence microscopy to directly elucidate the regulatory role of NCOA4 in ferritin autophagy and iron overload in 20% CS-induced cell damage. These findings indicated that ferritinophagy was involved in the development of VILI, and treatment with 3-MA and NCOA4 knockdown inhibited these processes. However, we did not investigate the role of other types of autophagy in promoting VILI-induced ferroptosis.

Another significant finding was that exposure to HTV or 20% CS for 4 h resulted in the activation of the AMPK/ULK1 pathway, which subsequently triggered ferritinophagy. Autophagy is a normal physiological process involved in cellular homeostasis and survival in normal cells. It plays an indispensable role in lung diseases [47, 48]. Phosphorylation of AMPK at Thr172 can modulate the phosphorylation of ULK1 at Ser555, which is a key modulator of autophagy [37, 49]. The AMPK/ULK1 axis can regulate autophagy in various diseases [50, 51]. However, whether the AMPK/ULK1 axis is involved in ferritinophagy in VIIL has not been elucidated. Therefore, we detected the protein expression levels of p-AMPK, p-ULK1, NCOA4, and FTH1. We found that compound C, inhibition of AMPK, can regulate NCOA4 and FHT1. Our results also showed that compound C alleviated lung injury and ameliorated cell damage, characterized by decreased lung tissue damage and lower levels of inflammatory cytokines. Our study demonstrated that activation of the AMPK/ULK1 signaling axis promotes ferritinophagy and subsequently induces ferroptosis in lung epithelial cells subjected to ventilator-induced injury.

While the findings of this study provide valuable insights into the relationship between ferritinophagy and VILI. It is important to acknowledge several limitations that necessitate further investigation. Firstly, the MLE12 cell, which is a key representative of resident alveolar cells, is abundant in iron ions and plays a vital role in iron metabolism. Nevertheless, it remains uncertain whether alveolar macrophages and other types of lung cells also undergo ferroptosis in the setting of VILI, and the underlying regulatory mechanisms have not yet been fully deciphered. Secondly, although the AMPK/ULK1 pathway has been extensively studied in the context of autophagy research, the relationship between its downstream components, such as LC3, ATG7, ATG5, and BECN1, and ferritinophagy remains unexplored and requires further investigation. Lastly, glutathione (GSH) and ferritin play a crucial role in ferroptosis. Although we utilized a range of indicators to indirectly assess potential alterations in these molecules, it is acknowledged that these methods may not fully capture the true levels of GSH and ferritin, subsequent research should directly measure levels of glutathione GSH and ferritin. Therefore, to validate these limitations and gain a deeper understanding of the complex mechanisms involved, future research must undertake more experimental exploration. This will not only help solidify our current understanding but also uncover new insights into the relationships between ferritinophagy, ferroptosis, and VILI across different lung cell types, including alveolar macrophages.

Conclusions

Ferroptosis is enhanced by the activation of NCOA4-mediated ferritinophagy in ventilator-induced lung epithelial cell damage. Activation of the AMPK/ULK1 pathway is involved in this process.

Supplementary Information

The online version contains supplementary material available at https://doi.org/10.1186/s12931-024-03076-7.

Supplementary Material 1

Acknowledgements

We would like to express our gratitude to Figdraw (https://www.figdraw.com/) for graphical abstract and EditSprings (https://www.editsprings.com/) for the expert linguistic services provided.

Author contributions

Huajin Ou and Jinyuan Lin designed all the experiments. Huajin Ou, Jinyuan Lin and Liu Ji performed the major experiments and drafted the manuscript. Liu Ye, Maoyao Ling, Xiaoting Liao and Fei Lin contributed the data analysis and contributed reagents and materials. Yuqing Wang, Bijun Luo and Zhaokun Hu supplement the experiments. Linghui Pan designed the overall study and determined the final version. All the authors have approved the manuscript and agreed submission to the esteemed journal. There are no conflicts of interest to declare.

Funding

This work was supported by Guangxi Clinical Research Center for Anesthesiology (GKAD22035214), the National Natural Science Foundation of China (82100091), Innovation Project of Guangxi Graduate Education (YCSW2024257), Youth Program of Scientific Research Foundation of Guangxi Medical Cancer Hospital (YQJ2022-4, YQJ2023-4), Youth Science Foundation of Guangxi Medical University (GXMUYSF202305).

Data availability

No datasets were generated or analysed during the current study.

Declarations

Ethics approval

Animal studies were reviewed and approved by the Institutional Animal Care and Use Committee of Guangxi Medical University Cancer Hospital.

Consent to participate
Not applicable.

Competing interests
The authors declare no competing interests.

Received: 4 October 2024 / Accepted: 18 December 2024
Published online: 24 December 2024

References

1. Bellani G, Laffey JG, Pham T, Fan E, Brochard L, Esteban A, Gattinoni L, van Haren F, Larsson A, McAuley DF, et al. Epidemiology, patterns of Care, and mortality for patients with Acute Respiratory Distress Syndrome in Intensive Care Units in 50 countries. JAMA. 2016;315:788–800.
2. Mart MF, Ware LB. The long-lasting effects of the acute respiratory distress syndrome. Expert Rev Respir Med. 2020;14:577–86.
3. Battaglini D, Fazzini B, Silva PL, Cruz FF, Ball L, Robba C, et al. Challenges in ARDS definition, management, and identification of effective personalized therapies. J Clin Med. 2023;12(4):1381. https://doi.org/10.3390/jcm12041381. PMID: 36835919; PMCID: PMC9967510.
4. Yamamoto R, Okazaki SR, Fujita Y, Seki N, Kokei Y, Sekine S, Wada S, Norisue Y, Narita C. Usefulness of low tidal volume ventilation strategy for patients with acute respiratory distress syndrome: a systematic review and meta-analysis. Sci Rep. 2022;12:9331.
5. Slutsky AS, Ranieri VM. Ventilator-induced lung injury. N Engl J Med. 2013;369:2126–36.
6. Roca O, Telias I, Grieco DL. Bedside-available strategies to minimise P-SILI and VILI during ARDS. Intensive Care Med. 2024;50:597–601.
7. Dixon SJ, Lemberg KM, Lamprecht MR, Skouta R, Zaitsev EM, Gleason CE, Patel DN, Bauer AJ, Cantley AM, Yang WS, et al. Ferroptosis: an iron-dependent form of nonapoptotic cell death. Cell. 2012;149:1060–72.
8. Chen X, Kang R, Kroemer G, Tang D. Ferroptosis in infection, inflammation, and immunity. J Exp Med. 2021;218(6):e20210518. https://doi.org/10.1084/jem.20210518. Epub 2021 May 12. PMID: 33978684; PMCID: PMC8126980.
9. Du J, Yu L, Yang X, Shao F, Xia J, Jin W, Zhang Y, Lei G, Wang Y, Li Y, Zhang J. Regulation of NCOA4-mediated iron recycling ameliorates paraquat-induced lung injury by inhibiting ferroptosis. Cell Commun Signal. 2024;22:146.
10. Wang K, Xu H, Zou R, Zeng G, Yuan Y, Zhu X, Zhao X, Li J, Zhang L. PCYT1A deficiency disturbs fatty acid metabolism and induces ferroptosis in the mouse retina. BMC Biol. 2024;22:134.
11. Wang X, Chen X, Zhou W, Men H, Bao T, Sun Y, Wang Q, Tan Y, Keller BB, Tong Q, et al. Ferroptosis is essential for diabetic cardiomyopathy and is prevented by sulforaphane via AMPK/NRF2 pathways. Acta Pharm Sin B. 2022;12:708–22.
12. Yu F, Zhang Q, Liu H, Liu J, Yang S, Luo X, Liu W, Zheng H, Liu Q, Cui Y, et al. Dynamic O-GlcNAcylation coordinates ferritinophagy and mitophagy to activate ferroptosis. Cell Discov. 2022;8:40.
13. Yang WS, SriRamaratnam R, Welsch ME, Shimada K, Skouta R, Viswanathan VS, Cheah JH, Clemons PA, Shamji AF, Clish CB, et al. Regulation of ferroptotic cancer cell death by GPX4. Cell. 2014;156:317–31.
14. Ganz T, Nemeth E. Iron homeostasis in host defence and inflammation. Nat Rev Immunol. 2015;15:500–10.
15. Mancias JD, Wang X, Gygi SP, Harper JW, Kimmelman AC. Quantitative proteomics identifies NCOA4 as the cargo receptor mediating ferritinophagy. Nature. 2014;509:105–9.
16. Santana-Codina N, Mancias JD. The role of NCOA4-mediated ferritinophagy in health and disease. Pharmaceuticals (Basel). 2018 ;11(4):114. https://doi.org/10.3390/ph11040114. PMID: 30360520; PMCID: PMC6316710.
17. Ling M, Ye L, Zeng Q, Li Z, He S, Lin J, Mo J, Pan L. Ferrostatin-1 alleviates ventilator-induced lung injury by inhibiting ferroptosis. Int Immunopharmacol. 2023;120:110356.
18. Lin J, Ou H, Luo B, Ling M, Lin F, Cen L, et al. Capsaicin mitigates ventilator-induced lung injury by suppressing ferroptosis and maintaining mitochondrial redox homeostasis through SIRT3-dependent mechanisms. Mol Med. 2024;30:148.
19. Xu W, Deng H, Hu S, Zhang Y, Zheng L, Liu M, Chen Y, Wei J, Yang H, Lv X. Role of ferroptosis in Lung diseases. J Inflamm Res. 2021;14:2079–90.
20. Yang S, Zhang T, Ge Y, Cheng Y, Yin L, Pu Y, Chen Z, Liang G. Ferritinophagy mediated by oxidative stress-driven mitochondrial damage is involved in the Polystyrene nanoparticles-Induced ferroptosis of Lung Injury. ACS Nano. 2023;17:24988–5004.
21. Li B, Wang W, Li Y, Wang S, Liu H, Xia Z, Gao W, Zhao B. cGAS-STING pathway aggravates early cerebral ischemia-reperfusion injury in mice by activating NCOA4-mediated ferritinophagy. Exp Neurol. 2023;359:114269.
22. Li N, Wang W, Zhou H, Wu Q, Duan M, Liu C, Wu H, Deng W, Shen D, Tang Q. Ferritinophagy-mediated ferroptosis is involved in sepsis-induced cardiac injury. Free Radic Biol Med. 2020;160:303–18.
23. Herzig S, Shaw RJ. AMPK: guardian of metabolism and mitochondrial homeostasis. Nat Rev Mol Cell Biol. 2018;19:121–35.
24. Kundu M, Lindsten T, Yang CY, Wu J, Zhao F, Zhang J, Selak MA, Ney PA, Thompson CB. Ulk1 plays a critical role in the autophagic clearance of mitochondria and ribosomes during reticulocyte maturation. Blood. 2008;112:1493–502.
25. Qin X, Zhang J, Wang B, Xu G, Yang X, Zou Z, Yu C. Ferritinophagy is involved in the zinc oxide nanoparticles-induced ferroptosis of vascular endothelial cells. Autophagy. 2021;17:4266–85.
26. Bao L, Zhao C, Feng L, Zhao Y, Duan S, Qiu M, Wu K, Zhang N, Hu X, Fu Y. Ferritinophagy is involved in Bisphenol A-induced ferroptosis of renal tubular epithelial cells through the activation of the AMPK-mTOR-ULK1 pathway. Food Chem Toxicol. 2022;163:112909.
27. Yue D, Zhang Q, Zhang J, Liu W, Chen L, Wang M, Li R, Qin S, Song X, Ji Y. Diesel exhaust PM2.5 greatly deteriorates fibrosis process in pre-existing pulmonary fibrosis via ferroptosis. Environ Int. 2023;171:107706.
28. Slavin SA, Leonard A, Grose V, Fazal F, Rahman A. Autophagy inhibitor 3-methyladenine protects against endothelial cell barrier dysfunction in acute lung injury. Am J Physiol Lung Cell Mol Physiol. 2018;314:L388–96.
29. Wang K, Zhao A, Tayier D, Tan K, Song W, Cheng Q, Li X, Chen Z, Wei Q, Yuan Y, Yang Z. Activation of AMPK ameliorates acute severe pancreatitis by suppressing pancreatic acinar cell necroptosis in obese mice models. Cell Death Discov. 2023;9:363.
30. Ye L, Zeng Q, Dai H, Zhang W, Wang X, Ma R, Hong X, Zhao C, Pan L. Endoplasmic reticulum stress is involved in ventilator-induced lung injury in mice via the IRE1α-TRAF2-NF-κB pathway. Int Immunopharmacol. 2020;78:106069.
31. Liao X, Zhang W, Dai H, Jing R, Ye M, Ge W, Pei S, Pan L. Neutrophil-derived IL-17 promotes Ventilator-Induced Lung Injury via p38 MAPK/MCP-1 pathway activation. Front Immunol. 2021;12:768813.
32. Matute-Bello G, Downey G, Moore BB, Groshong SD, Matthay MA, Slutsky AS, Kuebler WM. An official American Thoracic Society workshop report: features and measurements of experimental acute lung injury in animals. Am J Respir Cell Mol Biol. 2011;44:725–38.
33. Kulkarni HS, Lee JS, Bastarache JA, Kuebler WM, Downey GP, Albaiceta GM, Altemeier WA, Artigas A, Bates JHT, Calfee CS, et al. Update on the features and measurements of experimental Acute Lung Injury in animals: an official American thoracic Society Workshop Report. Am J Respir Cell Mol Biol. 2022;66:e1–14.
34. Jing R, Hu ZK, Lin F, He S, Zhang SS, Ge WY, Dai HJ, Du XK, Lin JY, Pan LH. Mitophagy-mediated mtDNA release aggravates stretching-Induced inflammation and lung epithelial cell Injury via the TLR9/MyD88/NF-κB pathway. Front Cell Dev Biol. 2020;8:819.
35. Hirayama T, Nagasawa H. Chemical tools for detecting Fe ions. J Clin Biochem Nutr. 2017;60:39–48.
36. Arosio P, Ingrassia R, Cavadini P. Ferritins: a family of molecules for iron storage, antioxidation and more. Biochim Biophys Acta. 2009;1790:589–99.
37. Kim J, Kundu M, Viollet B, Guan KL. AMPK and mTOR regulate autophagy through direct phosphorylation of Ulk1. Nat Cell Biol. 2011;13:132–41.
38. Curley GF, Laffey JG, Zhang H, Slutsky AS. Biotrauma and Ventilator-Induced Lung Injury: clinical implications. Chest. 2016;150:1109–17.
39. Wilcox ME, Maas MB. Beating the clock in ventilator-induced Lung Injury. Am J Respir Crit Care Med. 2023;207:1415–6.
40. Cressoni M, Gotti M, Chiurazzi C, Massari D, Algieri I, Amini M, Cammaroto A, Brioni M, Montaruli C, Nikolla K, et al. Mechanical power and development of ventilator-induced Lung Injury. Anesthesiology. 2016;124:1100–8.
41. Siempos II, Ma KC, Imamura M, Baron RM, Fredenburgh LE, Huh JW, Moon JS, Finkelsztein EJ, Jones DS, Lizardi MT et al. RIPK3 mediates pathogenesis of experimental ventilator-induced lung injury. JCI Insight 2018;3.
42. Fan S, He J, Yang Y, Wang D. Intermedin reduces oxidative stress and apoptosis in Ventilator-Induced Lung Injury via JAK2/STAT3. Front Pharmacol. 2021;12:817874.
43. Ge X, Sun J, Fei A, Gao C, Pan S, Wu Z. Hydrogen sulfide treatment alleviated ventilator-induced lung injury through regulation of autophagy and endoplasmic reticulum stress. Int J Biol Sci. 2019;15:2872–84.
44. Latunde-Dada GO. Ferroptosis: role of lipid peroxidation, iron and ferritinophagy. Biochim Biophys Acta Gen Subj. 2017;1861:1893–900.

45. Masaldan S, Clatworthy SAS, Gamell C, Meggyesy PM, Rigopoulos AT, Haupt S, Haupt Y, Denoyer D, Adlard PA, Bush AI, Cater MA. Iron accumulation in senescent cells is coupled with impaired ferritinophagy and inhibition of ferroptosis. Redox Biol. 2018;14:100–15.
46. Xu W, Wu Y, Wang S, Hu S, Wang Y, Zhou W, Chen Y, Li Q, Zhu L, Yang H, Lv X. Melatonin alleviates septic ARDS by inhibiting NCOA4-mediated ferritinophagy in alveolar macrophages. Cell Death Discov. 2024;10:253.
47. Racanelli AC, Kikkers SA, Choi AMK, Cloonan SM. Autophagy and inflammation in chronic respiratory disease. Autophagy. 2018;14:221–32.
48. Painter JD, Galle-Treger L, Akbari O. Role of autophagy in lung inflammation. Front Immunol. 2020;11:1337.
49. Kim YM, Kim MY, Kim HJ, Roh GS, Ko GH, Seo HG, Lee JH, Chang KC. Compound C independent of AMPK inhibits ICAM-1 and VCAM-1 expression in inflammatory stimulants-activated endothelial cells in vitro and in vivo. Atherosclerosis. 2011;219:57–64.
50. Zhang S, Xie Y, Yan F, Zhang Y, Yang Z, Chen Z, Zhao Y, Huang Z, Cai L, Deng Z. Negative pressure wound therapy improves bone regeneration by promoting osteogenic differentiation via the AMPK-ULK1-autophagy axis. Autophagy. 2022;18:2229–45.
51. Lu QB, Ding Y, Liu Y, Wang ZC, Wu YJ, Niu KM, Li KX, Zhang JR, Sun HJ. Metrnl ameliorates diabetic cardiomyopathy via inactivation of cGAS/STING signaling dependent on LKB1/AMPK/ULK1-mediated autophagy. J Adv Res. 2023;51:161–79.

Publisher's note